

Autoignition of Methyl Valerate at Low to Intermediate Temperatures and Elevated Pressures in a Rapid Compression Machine

Bryan W. Weber^{a,*}, Justin Bunnell^a, Kamal Kumar^b, Chih-Jen Sung^a

^a*Department of Mechanical Engineering, University of Connecticut, Storrs, CT, USA*

^b*Department of Mechanical Engineering, University of Idaho, Moscow, ID, USA*

Abstract

Methyl valerate ($\text{C}_6\text{H}_{12}\text{O}_2$, methyl pentanoate) is a methyl ester and a relevant surrogate component for biodiesel. In this work, we present ignition delays of methyl valerate measured using a rapid compression machine at a range of engine-relevant temperature, pressure, and equivalence ratio conditions. The conditions we have studied include equivalence ratios from 0.25 to 2.0, temperatures between 680 K and 1050 K, and pressures of 15 bar and 30 bar. The ignition delay data demonstrate a negative temperature coefficient region in the temperature range of 720 K–800 K for both $\phi = 2.0$, 15 bar and $\phi = 1.0$, 30 bar, with two-stage ignition apparent over the narrower temperature ranges of 720 K–760 K for the lower pressure and 740 K–760 K at the higher pressure. In addition, the experimental ignition delay data are compared with simulations using an existing chemical kinetic model from the literature. The simulations with the literature model under-predict the data by factors between 2 and 10 over the entire range of the experimental data. To help determine the possible reasons for the discrepancy between simulations and experiments, a new chemical kinetic model is developed using the Reaction Mechanism Generator (RMG) software. The agreement between the experimental data and the RMG model is improved but still not satisfactory. Directions for future improvement of the methyl valerate model are discussed.

*Corresponding Author: bryan.weber@uconn.edu

Keywords: chemical kinetics, rapid compression machine, autoignition, methyl ester

1. Introduction

For transportation applications, biodiesel is an important constituent in improving environmental friendliness of fuels. This is due to its renewability when produced from sustainable agricultural crops and its ability to reduce emissions relative to conventionally fueled engines [1]. Biodiesel typically consists of long-chain methyl ester molecules, with typical compositions of C_{14} to C_{20} [1]. Recognizing that the large molecular size of the methyl esters within biodiesel fuel makes creating and using detailed chemical kinetic mechanisms challenging [2], it is desired to study their combustion chemistry by studying simpler molecules.

A recent review paper summarizes the work on methyl esters relevant to biodiesel combustion [3]; the following summary focuses on ignition delay measurements, since these are the focus of this paper. Autoignition of methyl butanoate (MB, $C_5H_{10}O_2$) has been well-studied in both shock tube and rapid compression machine experiments [4, 5, 6, 7, 8, 9, 10]. The prevalence of MB data in the literature is largely due to the early identification of MB as a potential surrogate fuel for biodiesel [11]. However, the experiments have shown that MB may not be an appropriate surrogate for biodiesel, due to its lack of negative temperature coefficient (NTC) behavior, a requirement for a suitable biodiesel surrogate [3].

Larger methyl esters such as methyl valerate (MV, $C_6H_{12}O_2$, methyl pentanoate) have also been studied as possible biodiesel surrogates. Hadj-Ali et al. [9] used a rapid compression machine (RCM) to study the autoignition of several methyl esters including MV. Although MV exhibited two-stage ignition in this study, little additional research has been done on its oxidation. Korobeinichev et al. [12] studied MV in premixed laminar flames and extended a detailed high temperature chemical kinetic model to include MV and methyl hexanoate.

28 Dmitriev et al. [13] added MV to n-heptane/toluene fuel blends to determine
 29 the resulting intermediate species in premixed flames using a flat burner at
 30 1 atm and an equivalence ratio of 1.75. The addition of MV helped reduce soot
 31 forming intermediates including benzene, cyclopentadienyl, acetylene, propargyl,
 32 and vinylacetylene [13]. Hayes and Burgess [14] computationally examined
 33 the peroxy radical isomerization reactions for MV to better understand the low
 34 temperature reaction pathways. Finally, Diévar et al. [15] used diffusion flames
 35 in the counterflow configuration to determine extinction limits for a number of
 36 methyl esters, including MV, and validated a detailed kinetic model with the
 37 experimental data.

38 This work provides additional data for the autoignition of MV. Data is col-
 39 lected in a RCM under engine relevant conditions spanning from 15 bar to 30 bar,
 40 equivalence ratios from 0.25 to 2.0, and temperatures from 682 K to 1048 K. The
 41 NTC region of MV is mapped out to provide additional information on the fi-
 42 delity of using MV as a biodiesel surrogate.

43 **2. Experimental Methods**

44 The RCM used in this study is a single piston arrangement and is pneu-
 45 matically driven and hydraulically stopped. The device has been described in
 46 detail previously [16] and will be described here briefly for reference. The end
 47 of compression (EOC) temperature and pressure (T_C and P_C respectively), are
 48 independently changed by varying the overall compression ratio, initial pressure
 49 (P_0), and initial temperature (T_0) of the experiments. The piston in the re-
 50 action chamber is machined with a specially designed crevice to suppress the
 51 roll-up vortex effect and promote homogeneous conditions in the reactor during
 52 and after compression [17].

53 The primary diagnostic on the RCM is the in-cylinder pressure measured by
 54 a Kistler 6125C dynamic transducer that is compensated for thermal shock. The
 55 transducer is coupled to a Kistler 5010B charge amplifier. The voltage output
 56 of the charge amplifier is recorded by a National Instruments 9125 analog input

57 device connected to a cDAQ 9178 chassis. The voltage is sampled at a rate
58 of either 50 kHz or 100 kHz by a LabView VI and processed by a Python
59 package called UConnRCMPy [18]. Version 3.0.0 of UConnRCMPy [19], 3.6.1
60 of Python, 2.3.0 of Cantera [20], 1.13 of NumPy [21], 0.19.0 of SciPy [22], and
61 2.0.1 of Matplotlib [23] were used in the analysis in this paper.

Check this

62 The compression stroke of the RCM brings the fuel/oxidizer mixture to the
63 EOC conditions, and for suitable thermodynamic states, the mixture will ignite
64 after a delay period. The definitions of the ignition delays are shown in Fig. 1.
65 The time of the EOC is defined as the maximum of the pressure trace prior to
66 the start of ignition and the ignition delays are defined as the time from the EOC
67 until local maxima in the first time derivative of the pressure. Each experimental
68 condition is repeated at least five times to ensure repeatability of the data. As
69 there is some random scatter present in the data, the standard deviation (σ) of
70 the ignition delays from the runs at a given condition is computed. In all cases,
71 σ is less than 10 % of the mean value of the overall ignition delay.

72 In addition to the reactive experiments, non-reactive experiments are con-
73 ducted to determine the influence of machine-specific behavior on the experi-
74 mental conditions and permit the calculation of the EOC temperature via the
75 isentropic relations between pressure and temperature [24]. The EOC temper-
76 ature is calculated by the procedure described in Section 3.

77 The mixtures considered in this study are shown in Table 1. Four equivalence
78 ratios of MV in “air” are considered. The ratio of Ar : N₂ in the oxidizer is
79 varied to adjust the temperatures reached at the EOC for a given mixture. Two
80 P_C conditions are studied in this work, 15 bar and 30 bar, representing engine-
81 relevant conditions. For the $\phi = 2.0$ condition, only $P_C = 15$ bar is considered
82 because we could not achieve T_C values low enough that the ignition was long
83 enough to be measured in our apparatus (the typical lower limit of ignition delay
84 on the present RCM is approximately 5 ms).

85 Mixtures are prepared in stainless steel mixing tanks, approximately 17 L
86 and 15 L in size. The proportions of reactants in the mixture are determined
87 by specifying the absolute mass of the fuel, the equivalence ratio (ϕ), and the

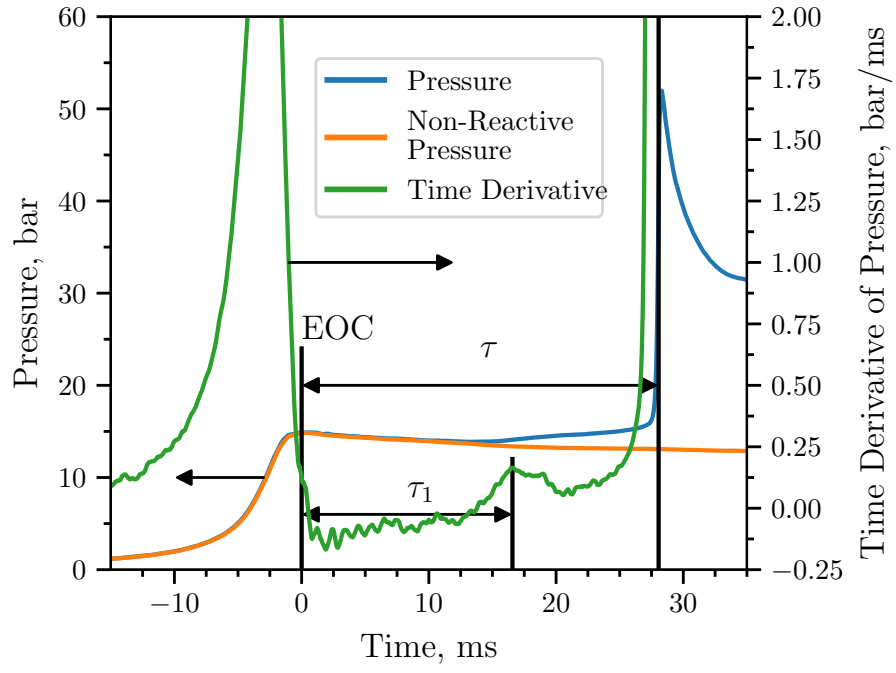


Figure 1: Definition of the ignition delays used in this work. The experiment in this figure was conducted for a $\phi = 2.0$ mixture with $\text{Ar}/(\text{N}_2 + \text{Ar}) = 0.5$, $P_0 = 0.7694$ bar, $T_0 = 373$ K, $P_C = 14.94$ bar, $T_C = 723$ K, $\tau = (27.44 \pm 0.99)$ ms, $\tau_1 = (16.57 \pm 0.48)$ ms.

Table 1: Mixtures considered in this work

ϕ	Mole Fraction (purity)				Ar/(N ₂ + Ar)
	MV (100 %)	O ₂ (99.994 %)	Ar (99.999 %)	N ₂ (99.999 %)	
0.25	0.0065	0.2087	0.7848	0.0000	1.0
0.5	0.0130	0.2074	0.7798	0.0000	1.0
1.0	0.0256	0.2047	0.7697	0.0000	1.0
1.0	0.0256	0.2047	0.3849	0.3848	0.5
2.0	0.0499	0.1996	0.0000	0.7505	0.0
2.0	0.0499	0.1996	0.3752	0.3753	0.5

ratio of Ar : N₂ in the oxidizer. Mixtures are made by first vacuuming the mixing tanks to an ultimate pressure less than 5 torr. Since MV is a liquid with a relatively small vapor pressure at room temperature and pressure, it is measured gravimetrically in a syringe to within 0.01 g of the specified value. The fuel is injected into the mixing tank through a septum. Proportions of O₂, Ar, and N₂ are added manometrically at room temperature and the total pressure is measured by an Omega Engineering MMA type static pressure transducer. The same transducer is used to measure the pressure of the reactants prior to an experiment.

The RCM is equipped with heaters to control the initial temperature of the mixture. After filling in the components to the mixing tanks, the heaters are switched on and the system is allowed 1.5 h to come to steady state. The mixing tanks are also equipped with magnetic stir bars so the reactants are well mixed for the duration of the experiments.

The initial temperature is chosen such that the saturated vapor pressure (P_{sat}) of the fuel at the initial temperature is at least twice the partial pressure of the fuel in the mixing tank. The Antoine equation

$$\log_{10} P_{\text{sat}} = A - \frac{B}{T - C} \quad (1)$$

is used to model the saturated vapor pressure of MV as a function of temper-

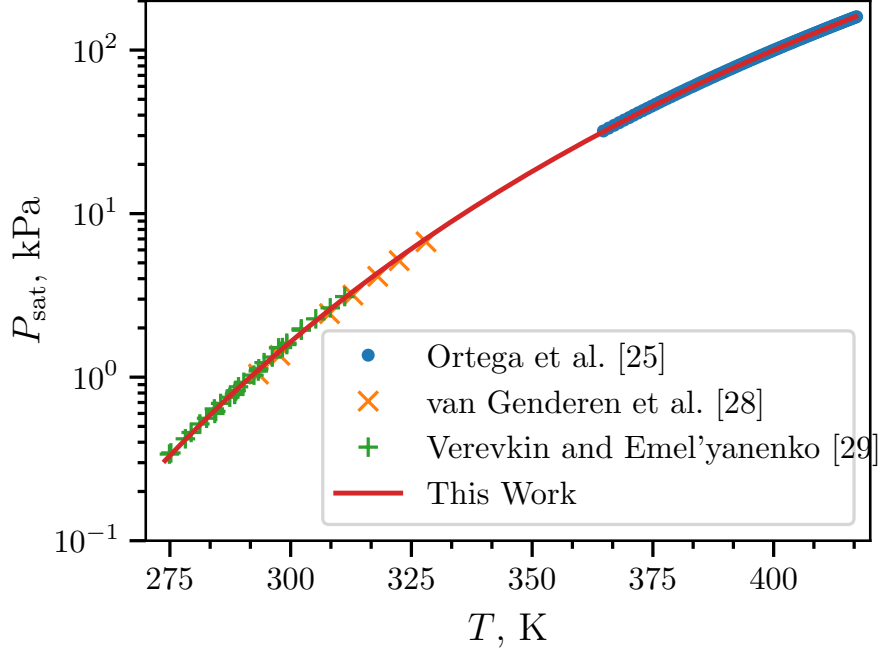


Figure 2: Saturated vapor pressure of MV as a function of temperature, plotted using the Antoine equation, Eq. (1), with $A = 6.4030$, $B = 1528.69$, and $C = 52.881$.

103 ature, where A , B , and C are substance-specific coefficients. Coefficients for
 104 Eq. (1) are given in the literature by Ortega et al. [25], Camacho et al. [26],
 105 and Stephenson et al. [27]; unfortunately, the values of the coefficients are dif-
 106 ferent among all three authors. Therefore, coefficients for use in Eq. (1) are
 107 determined in this work by least squares fitting of the data of Ortega et al.
 108 [25], van Genderen et al. [28], and Verevkin and Emel'yanenko [29] using the
 109 `curve_fit()` function of SciPy [22] version 0.19.0. Figure 2 shows that the coef-
 110 ficients fit with this procedure give good agreement with the experimental data;
 111 values for the coefficients computed in this work and in the literature works are
 112 given in Table 2. The data used to calculate the coefficients are provided in the
 113 Supplementary Material.

Table 2: Antoine Equation coefficients computed in this work and from the literature. The 2σ confidence interval is estimated by taking the square root of the diagonals of the covariance matrix returned from `curve_fit()`

	A	B	C	T_{\min} , K	T_{\max} , K
This Work	6.4030	1528.69	52.881	274.9	417.18
2σ Confidence Interval	0.0919	53.47	4.934	—	—
[25]	6.23175	1429.00	62.30	364.75	417.18
[26]	5.9644	1281.06	75.94	281	547
[27]	6.62646	1658.4	42.09	297	411

114 3. Computational Methods

115 3.1. RCM Modeling

116 The Python 3.6 interface of Cantera [20] version 2.3.0 is used for all sim-
117 ulations in this work. Detailed descriptions of the use of Cantera for these
118 simulations can be found in the work of Weber and Sung [18] and Dames et al.
119 [30]; a brief overview is given here. As mentioned in Section 2, non-reactive
120 experiments are conducted to characterize the machine-specific effects on the
121 experimental conditions in the RCM. This pressure trace is combined with the
122 reactive pressure trace and used to compute a volume trace by assuming that
123 the reactants undergo a reversible, adiabatic, constant composition (i.e., isen-
124 tropic) compression during the compression stroke and an isentropic expansion
125 after the EOC. The volume trace is applied to a simulation conducted in an
126 **IdealGasReactor** in Cantera [20] using the CVODES solver from the SUNDI-
127 ALS suite [31]. The ignition delay from the simulations is defined in the same
128 manner as in the experiments. The time derivative of the pressure in the sim-
129 ulations is computed by second order Lagrange polynomials, as discussed by
130 Chapra and Canale [32].

131 To the best of our knowledge, there are three mechanisms for MV combus-
132 tion available in the literature. The first two, by [12] and [13], were developed

133 to simulate flames, and do not include the low-temperature chemistry necessary
134 to simulate the conditions in these experiments. The third model was devel-
135 oped by [15] and includes low-temperature chemistry of MV, although it was
136 only validated by comparison with flame extinction limits. In converting this
137 mechanism for use in Cantera, we found that there were many species in the
138 thermodynamic database with multiple data entries. For most of these species
139 the thermodynamic data is identical. However, some species are not exact du-
140 plicates. For these species, it is not clear from the thermodynamic database file
141 which data set should be preferred. Since Cantera (and CHEMKIN) choose the
142 first instance of a duplicate species to be used, we retained the first entry for
143 all duplicated species. The detailed [15] model includes 1103 species and 7557
144 reactions, and the CHEMKIN and Cantera formatted input files are available
145 in the Supplementary Material.

check this

146 3.2. Reaction Mechanism Generator

147 In addition to using a mechanism from the literature, we investigate the use
148 of an automatic mechanism generator, the open-source Reaction Mechanism
149 Generator (RMG) [33] version 1.0.4. The Python version of RMG is used, which
150 requires Python 2.7, and version 1.10.0 of the RMG database is used. The final
151 RMG model contains 483 species and 19990 reactions. Note that the number
152 of species is much lower than the [15] model because the RMG model focuses
153 on only one fuel (MV), but the number of reactions is substantially higher.

154 4. Experimental Results

155 Figure 3 shows the ignition delay results measured in this study. Filled mark-
156 ers denote the overall ignition delay and hollow markers indicate the first-stage
157 ignition delay. Vertical error bars are drawn on the symbols to represent the
158 uncertainty in the ignition delay; for many of the experiments, the uncertainty
159 is approximately the same size as the data point, so the error bar is hidden.
160 Horizontal error bars are shown on the first and last points of each equivalence

ratio indicating the estimated uncertainty in the EOC temperature of $\pm 1\%$ [34]. Fig. 3a shows the results for a compressed pressure of 15 bar, while Fig. 3b shows the results for a compressed pressure of 30 bar. Note that $\phi = 2.0$ results were not collected for 30 bar, so there are no red data points in Fig. 3b.

It can be seen from Fig. 3 that the ignition delays for the $\phi = 0.25$ and 0.5 mixtures do not show an NTC region of the ignition delay for both of the pressures studied in this work. However, the $\phi = 1.0$ mixture shows an NTC region at $P_C = 30$ bar between approximately 720 K and 800 K, with measured first-stage ignition delays at 734 K and 757 K. In addition, the $\phi = 2.0$ mixture shows an NTC region of ignition delay at 15 bar from approximately 720 K to 775 K, with measured first-stage ignition delays between 720 K and 750 K.

Figure 4 shows the pressure traces for selected experiments at $\phi = 1.0$, $P_C = 30$ bar. The three reactive pressure traces shown are at the low-temperature end of the NTC (blue, 700 K), one case with two-stage ignition (orange, 734 K), and one case near the high-temperature limit of the NTC region (green, 775 K). Also shown is the non-reactive pressure trace for the 700 K case (red). By comparing the 700 K pressure trace with the non-reactive pressure trace, it can be seen that there is substantial heat release prior to main ignition as measured by the deviation of the reactive pressure trace from the non-reactive trace. However, there is only one peak in the time derivative of the pressure, so no first-stage ignition delay is defined for this case. It can also be seen in Fig. 4 that the 775 K case shows some heat release prior to ignition, although again there is only one peak in the time derivative of the pressure. Furthermore, the heat release at 775 K appears to be more gradual than at the lowest temperature.

5. Computational Results

Figure 5 compares experimentally measured overall ignition delays with ignition delays computed with the detailed model of [15] for the $\phi = 1.0$ experiments. Results for the other equivalence ratios are similar to these results, so are not shown here. It is important to note that the model of [15] was not validated

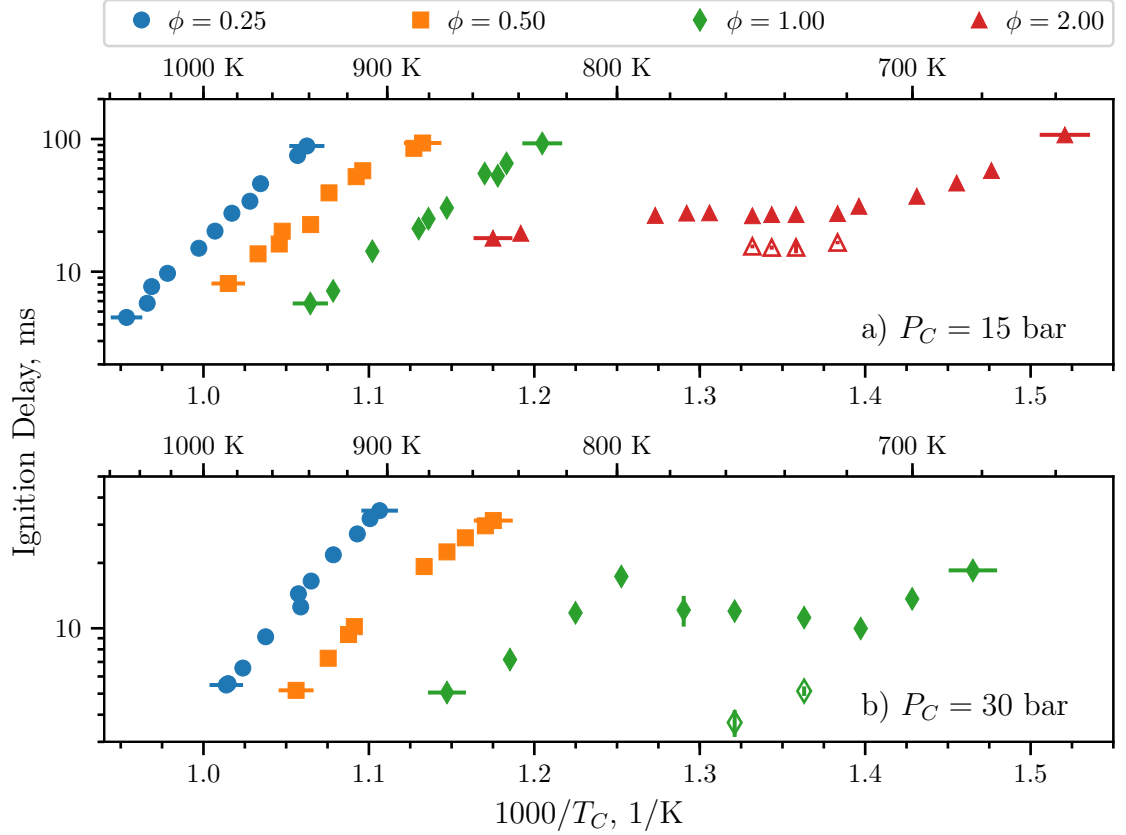


Figure 3: Ignition delays of MV as a function of inverse temperature. Filled points are the overall ignition delays and hollow points are the first stage ignition delays. a) 15 bar. b) 30 bar

for MV ignition delays, only for extinction strain rates. At 15 bar, the model tends to under-predict the ignition delay and predicts an NTC region that is not present in the experiments. At 30 bar, the model predicts the low-temperature ignition delays well, but does not predict the NTC region found experimentally.

To understand the underlying reasons for the disagreement between the [15] model and the data, we constructed an additional model using RMG (see Section 3.2). As can be seen in Fig. 5, the agreement between the RMG model and the experimental data is similar to the [15] model for the 30 bar data. At 15 bar, the RMG model predicts a somewhat longer ignition delay than the model of

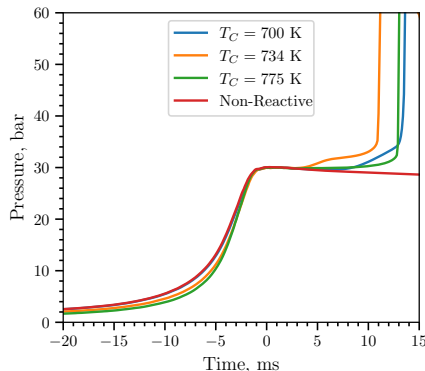


Figure 4: Selected pressure traces around the NTC region of ignition delay for $\phi = 1.0$

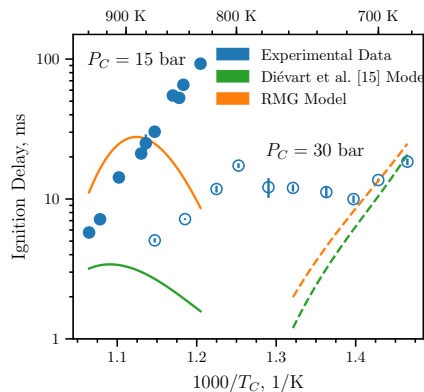


Figure 5: Comparison of experimental and simulated results for $\phi = 1.0$

[15], but still predicts an NTC region where none is present in the experimental data.

In general, there could be three likely sources of error in the models: missing reaction pathways, incorrect values of the reaction rates, and incorrect values for thermodynamic properties of the species. We have noted in Section 3.2 that the RMG model has many more reactions than the [15] model and the algorithm used in RMG considers a substantial number of the possible pathways. This reduces the possibility of missing reaction pathways affecting the model. Further detailed studies are required to ensure that the RMG model includes all of the relevant reaction pathways.

The second source of error may be incorrect reaction rate parameters, either because the rates are specified incorrectly in the model (e.g., typos) or because the rates are not well estimated by the typical analogy based-rules. It should be noted that errors of this type may affect the model generated by RMG—if the rates are not estimated correctly, reactions that are important in reality may not be included in the model. Determining the accuracy of the reaction rates used in the RMG and [15] models requires further detailed studies of the models. Another related source of error could be incorrect estimation of the pressure dependence of the reaction rates, which may be particularly important

218 for the isomerization reactions prevalent in low-temperature chemistry.

219 The third source of error may lie in the estimation of the thermodynamic
220 properties of the species, particularly their heats of formation. We have begun to
221 analyze the possibility of this source of error by conducting a reaction pathway
222 analysis to determine which radicals are formed from the breakdown of the fuel.
223 The following analysis is conducted for a constant volume simulation at 700 K,
224 30 bar, where the rates of production of the species have been integrated until
225 the time of 20 % fuel consumption. The results of this analysis are shown in
226 Fig. 6 and Table 3 for the two models. The percentages shown in the Table 3
227 are the percent of the fuel destroyed to form a particular fuel radical by all the
228 reactions that can form that radical.

229 At the relatively low temperature and high pressure condition of this analy-
230 sis, all of the fuel is destroyed by H-atom abstractions to form the fuel radicals
231 shown. It can be seen that the two models have quite different distributions of
232 products from the first H-abstraction reactions. The model of [15] predicts that
233 H-abstraction from the second carbon is the most prevalent, followed closely by
234 abstraction from the methyl group. This is in line with the bond energies of the
235 C-H bonds for those carbon atoms; we expect that the presence of the oxy-
236 gen atoms will cause hydrogen abstraction at the nearby carbons to be favored.
237 However, the RMG model predicts that radicals in the middle of the carbon
238 chain will be primarily formed. The cause of this discrepancy is under investi-
239 gation, but it may be caused by the estimation of thermodynamic properties of
240 the radicals.

241 6. Conclusions

242 In this study, we have measured ignition delays for methyl valerate over a
243 wide range of engine-relevant pressures, temperatures, and equivalence ratios.
244 An NTC region of the ignition delay and two-stage ignition were recorded for
245 pressures of 15 bar at $\phi = 2.0$ and 30 bar at $\phi = 1.0$. A detailed chemical ki-
246 netic model available in the literature was unable to reproduce the experimental

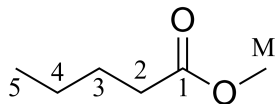


Figure 6: Structure of MV with carbon atoms labeled according to the convention used in Table 3

Table 3: Percent of MV destroyed to form fuel radical species with a hydrogen atom missing at the location indicated in the first column

Radical Site	[15] [%]	RMG Model [%]
2	29.3	7.4
3	17.5	36.0
4	17.5	41.1
5	9.4	3.7
M	26.3	11.8

247 results, so a new model was constructed using the Reaction Mechanism Gen-
 248 erator software. Although the new model contains many more reactions than
 249 the literature model, it is still unable to predict the experimental ignition de-
 250 lays satisfactorily. Possible reasons for the discrepancy include missing reaction
 251 pathways, incorrect rate estimates, and incorrect thermodynamic property esti-
 252 mates. Future work will include investigation of the discrepancies between mod-
 253 els and experiments to further understand the autoignition kinetics of methyl
 254 valerate.

255 References

- 256 [1] S. K. Hoekman, C. Robbins, Fuel Processing Technology 96 (2012) 237–249.
- 257 [2] J. Y. Lai, K. C. Lin, A. Violi, Progress in Energy and Combustion Science
 258 37 (2011) 1–14.
- 259 [3] L. Coniglio, H. Bennadji, P. Glaude, O. Herbinet, F. Billaud, Progress in
 260 Energy and Combustion Science 39 (2013) 340–382.
- 261 [4] W. K. Metcalfe, S. Dooley, H. J. Curran, J. M. Simmie, A. M. El-Nahas,
 262 M. V. Navarro, The Journal of Physical Chemistry A 111 (2007) 4001–4014.

- [5] S. M. Walton, M. S. Wooldridge, C. K. Westbrook, Proceedings of the Combustion Institute 32 (2009) 255–262.
- [6] S. Dooley, H. J. Curran, J. M. Simmie, Combustion and Flame 153 (2008) 2–32. 16.
- [7] B. Akih-Kumgeh, J. M. Bergthorson, Energy & Fuels 24 (2010) 2439–2448.
- [8] B. Akih-Kumgeh, J. M. Bergthorson, Combustion and Flame 158 (2011) 1037–1048.
- [9] K. Hadj-Ali, M. Crochet, G. Vanhove, M. Ribaucour, R. Minetti, Proceedings of the Combustion Institute 32 (2009) 239–246. 23.
- [10] K. Kumar, C.-J. Sung, Combustion and Flame 171 (2016) 1–14.
- [11] E. Fisher, W. J. Pitz, H. J. Curran, C. K. Westbrook, Proceedings of the Combustion Institute 28 (2000) 1579–1586. 10.
- [12] O. Korobeinichev, I. Gerasimov, D. Knyazkov, A. Shmakov, T. Bolshova, N. Hansen, C. K. Westbrook, G. Dayma, B. Yang, Zeitschrift für Physikalische Chemie 229 (2015).
- [13] A. M. Dmitriev, D. A. Knyazkov, T. A. Bolshova, A. G. Shmakov, O. P. Korobeinichev, Combustion and Flame 162 (2015) 1964–1975.
- [14] C. Hayes, D. R. Burgess, Proceedings of the Combustion Institute 32 (2009) 263–270. 26.
- [15] P. Diévert, S. H. Won, J. Gong, S. Dooley, Y. Ju, Proceedings of the Combustion Institute 34 (2013) 821–829.
- [16] G. Mittal, C.-J. Sung, Combustion Science and Technology 179 (2007) 497–530.
- [17] G. Mittal, C.-J. Sung, Combustion and Flame 145 (2006) 160–180.
- [18] B. W. Weber, C.-J. Sung, in: S. Benthall, S. Rostrup (Eds.), Proceedings of the 15th Python in Science Conference, pp. 36–44.

- 289 [19] B. W. Weber, R. Fang, C.-J. Sung, UConnRCMPy, 2017.
- 290 [20] D. G. Goodwin, H. K. Moffat, R. L. Speth, Cantera: An Object-oriented
291 Software Toolkit for Chemical Kinetics, Thermodynamics, and Transport
292 Processes, 2017.
- 293 [21] S. van der Walt, S. C. Colbert, G. Varoquaux, Computing in Science &
294 Engineering 13 (2011) 22–30.
- 295 [22] E. Jones, T. Oliphant, P. Peterson, others, SciPy: Open Source Scientific
296 Tools for Python, 2001-.
- 297 [23] J. D. Hunter, Computing in Science & Engineering 9 (2007) 90–95.
- 298 [24] D. Lee, S. Hochgreb, Combustion and Flame 114 (1998) 531–545.
- 299 [25] J. Ortega, F. Espiau, J. Tojo, J. Canosa, A. Rodríguez, Journal of Chemical
300 & Engineering Data 48 (2003) 1183–1190.
- 301 [26] A. G. Camacho, J. M. Moll, S. Canzonieri, M. A. Postigo, Journal of Chem-
302 ical & Engineering Data 52 (2007) 871–875.
- 303 [27] R. M. Stephenson, S. Malanowski, D. Ambrose, Handbook of the Thermo-
304 dynamics of Organic Compounds, Elsevier, New York, 1987.
- 305 [28] A. C. van Genderen, J. van Miltenburg, J. G. Blok, M. J. van Bommel,
306 P. J. van Ekeren, G. J. van den Berg, H. A. Oonk, Fluid Phase Equilibria
307 202 (2002) 109–120.
- 308 [29] S. P. Verevkin, V. N. Emel’yanenko, Fluid Phase Equilibria 266 (2008)
309 64–75.
- 310 [30] E. E. Dames, A. S. Rosen, B. W. Weber, C. W. Gao, C.-J. Sung, W. H.
311 Green, Combustion and Flame 168 (2016) 310–330.
- 312 [31] A. C. Hindmarsh, P. N. Brown, K. E. Grant, S. L. Lee, R. Serban, D. E.
313 Shumaker, C. S. Woodward, ACM Transactions on Mathematical Software
314 31 (2005) 363–396.

- 315 [32] S. C. Chapra, R. P. Canale, Numerical Methods for Engineers, McGraw-
316 Hill Higher Education, Boston, 6th ed edition, 2010.
- 317 [33] J. W. Allen, C. F. Goldsmith, W. H. Green, Physical Chemistry Chemical
318 Physics 14 (2012) 1131–1155.
- 319 [34] B. W. Weber, C.-J. Sung, M. W. Renfro, Combustion and Flame 162 (2015)
320 2518–2528.